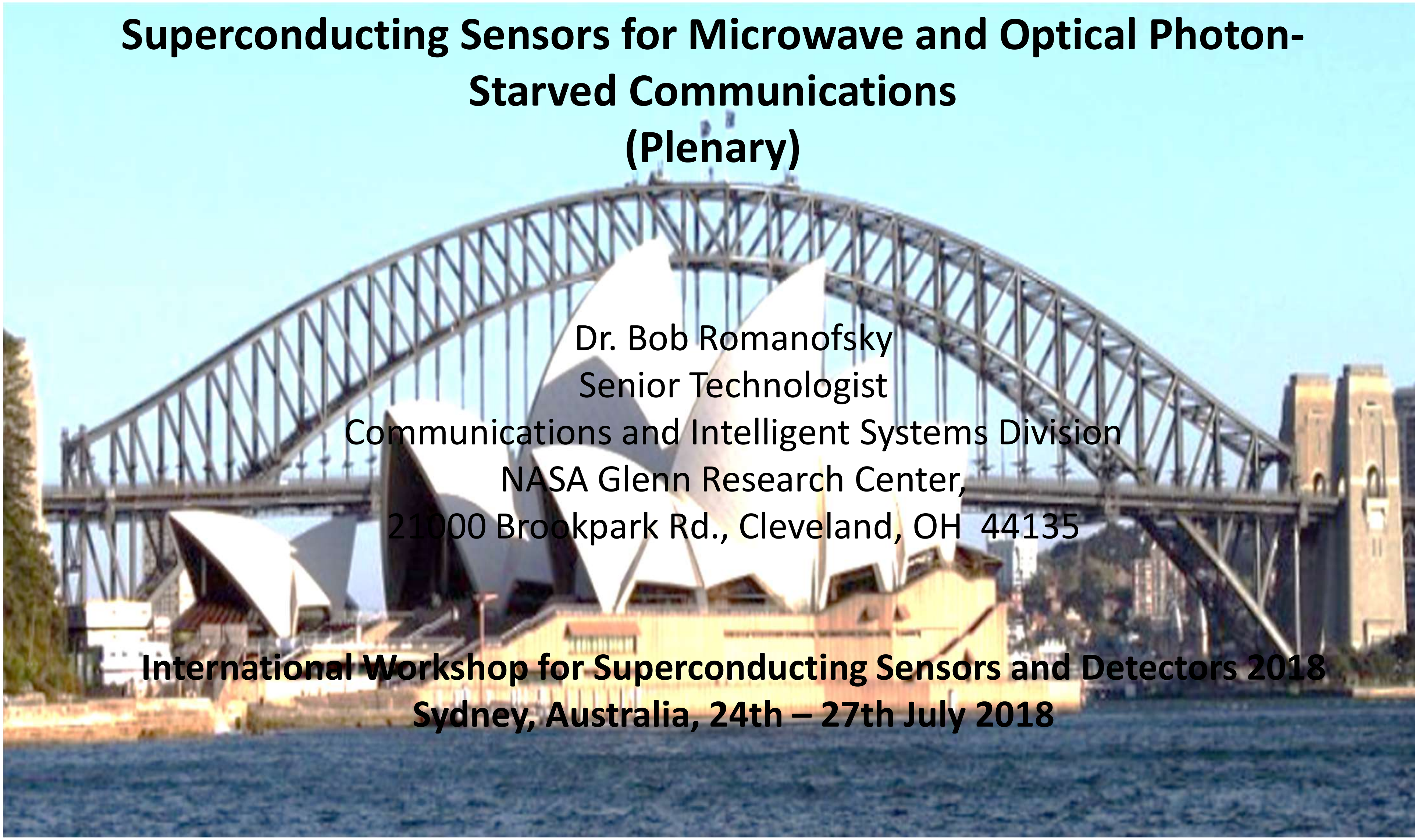

Superconducting Sensors for Microwave and Optical Photon-Starved Communications (Plenary)

Dr. Bob Romanofsky
Senior Technologist
Communications and Intelligent Systems Division
NASA Glenn Research Center,
21000 Brookpark Rd., Cleveland, OH 44135

International Workshop for Superconducting Sensors and Detectors 2018
Sydney, Australia, 24th – 27th July 2018

Outline

- NASA Glenn Research Center
    - Communications Research and Technology
- Deep Space Communications
    - Optical versus Microwave
- Kinetic Inductance Detectors
    - Subtle Aspects of Transmission Line Resonators
- Superconducting Quantum Interference [Filter] Receivers
    - A “Noiseless” Receiver?
- An Optical Ground Array Concept
    - An Economically Viable Alternative to a Large Monolithic Reflector

Glenn Research Center

Lewis Field

(Cleveland)

- **350 acres**
- **1626 civil servants and 1511 contractors**

Plum Brook Station Test Site

(Sandusky)

- **6500 acres**
- **11 civil servants and 102 contractors**

as of 1/2013

Glenn Core Competencies

Air-Breathing Propulsion

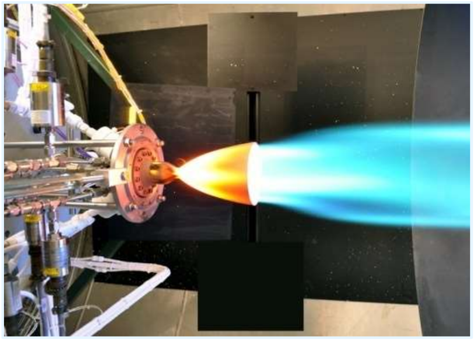

In-Space Propulsion and Cryogenic Fluids Management

Physical Sciences and Biomedical Technologies in Space

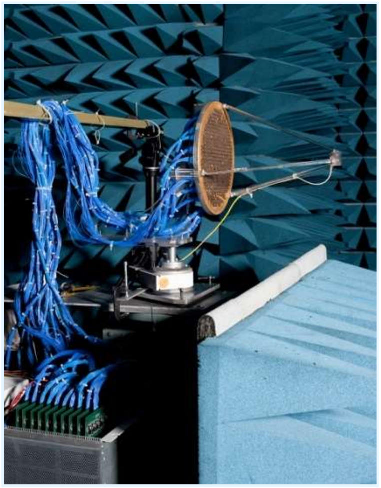

Communications Technology and Development

Power, Energy Storage and Conversion

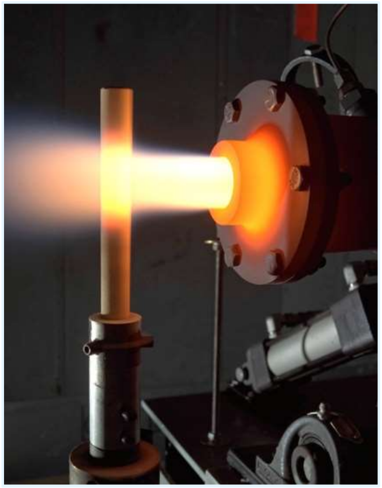

Materials and Structures for Extreme Environments

Communications Research and Technology

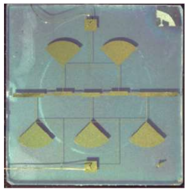

Fundamental Research
Materials and Devices

High Power Amplifiers

Software Defined Radio

Spaceflight Equipment
Development

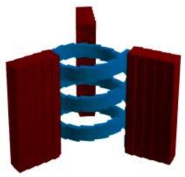

Simulation and Modeling

Cryogenic Electronics &
Superconductivity

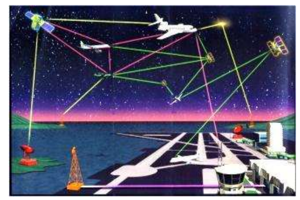

Aviation Safety and Security

Space Technology Hall of Fame
Advanced Communication Technology Satellite
Inflatable Antenna System

Laboratory Facilities

Architectures,
Network Protocols

Emmy Award
Depressed Collector Traveling Wave Tube
Communications Technology Satellite

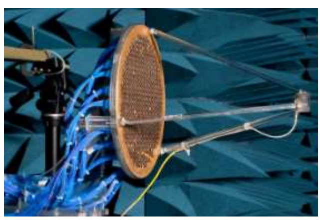

Phased Array Antennas

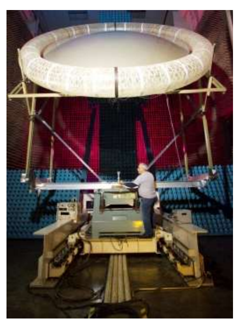

Deployable Antennas

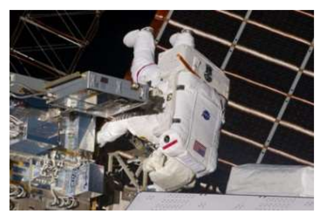

Space Flight Experiments

Cryogenic Electronics & Superconductivity Heritage in the Advanced High Frequency Branch

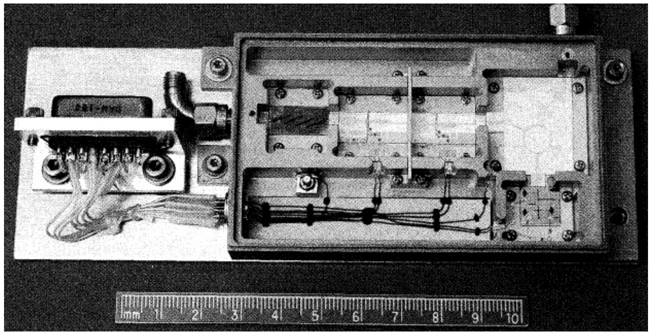

Space Qualified X-band Cryogenic Receiver Front end (NRL High Temperature Superconductivity Space Experiment)

1994

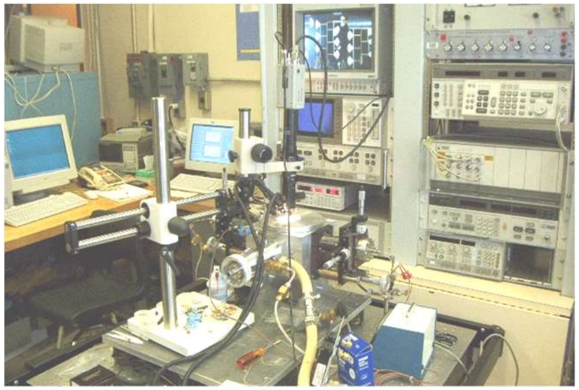

40 GHz Cryogenic On-Wafer Probe Station

1994

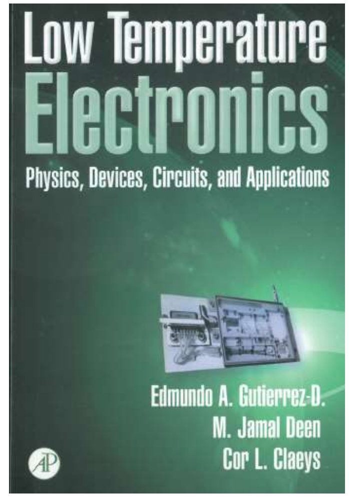

Chapter 7: Hybrid Superconductor/ Semiconductor Microwave Devices and Circuits

1996

Portable K-Band Cryogenically Cooled Low-Noise Receiver for the Direct Data Distribution Experiment

1999

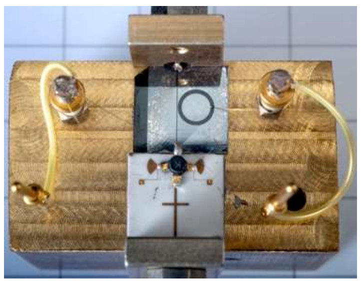

Ku-Band Ferroelectric/ YBaCuO Tunable Oscillator

2000

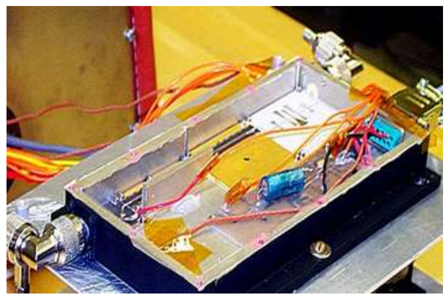

Space Shuttle Return-to-Flight GPS Receiver Cryogenic Characterization

2004

X-Band SQIF

2014

Increase of Date Rate as a Function of Time

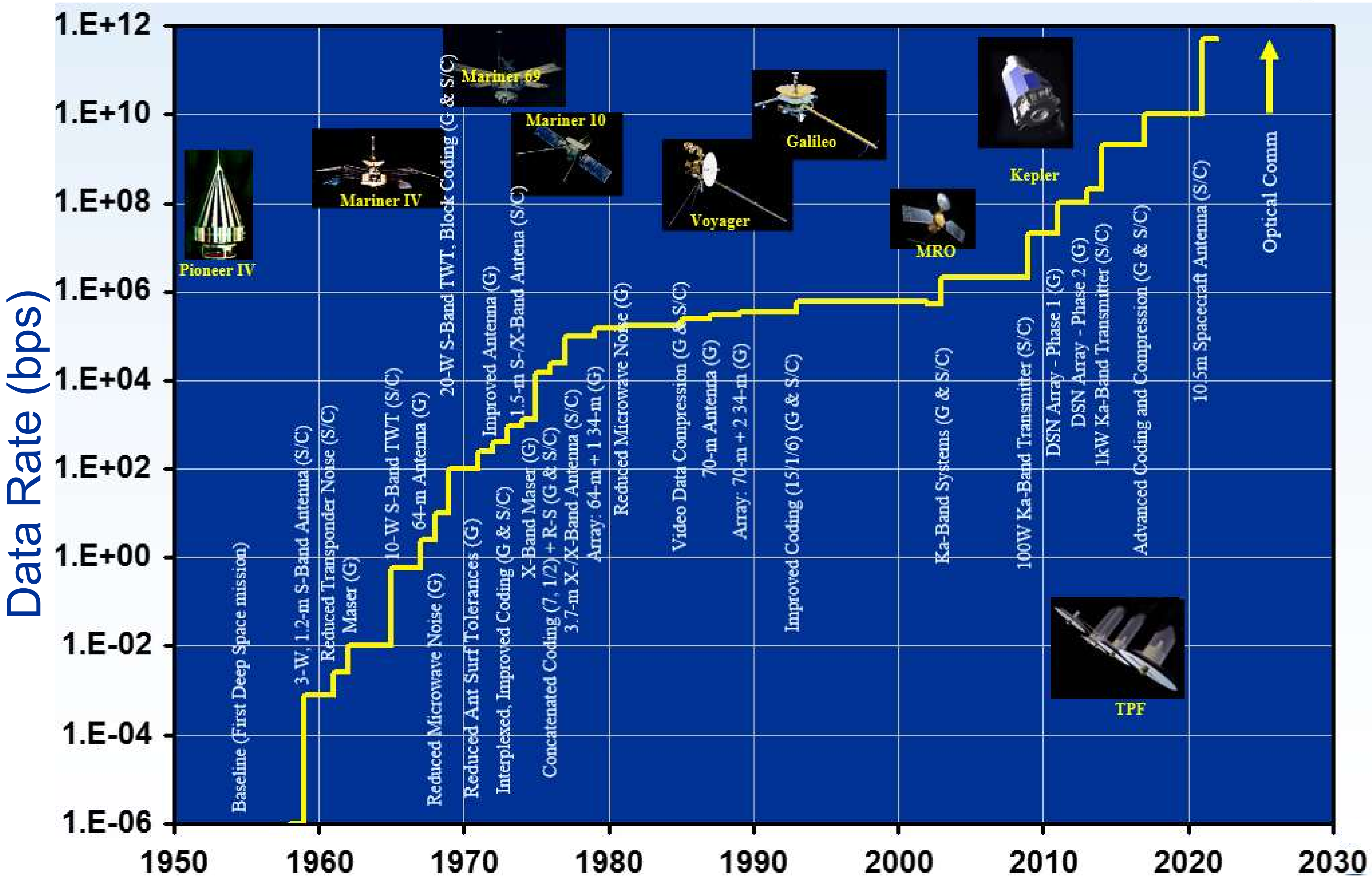

Background

- The highest data rate from deep space was achieved by the Mars Reconnaissance Orbiter at 6 Mb/s (X-band) from Mars at perigee.
- In October 2013 NASA's Lunar Laser Communication Demonstration (LLCD) hosted by the Lunar Atmosphere and Dust Environment Explorer mission demonstrated a downlink rate of 622 Mb/s from lunar range.
- Deep-Space optical communications differs from near earth communications because one-way link times can exceed 20 minutes (as opposed to a few seconds) and the great distances result in photon limited signals.
- NASA JPL's Deep Space Optical Communications project is developing technologies to enable an optical transceiver capable of 267 Mb/s at Mars perigee to a ≈12 m ground terminal.
- Large aperture ground telescopes will be equipped with low noise, high detection efficiency, single photon counting detectors.

Let's Compare Signals and Sensitivity

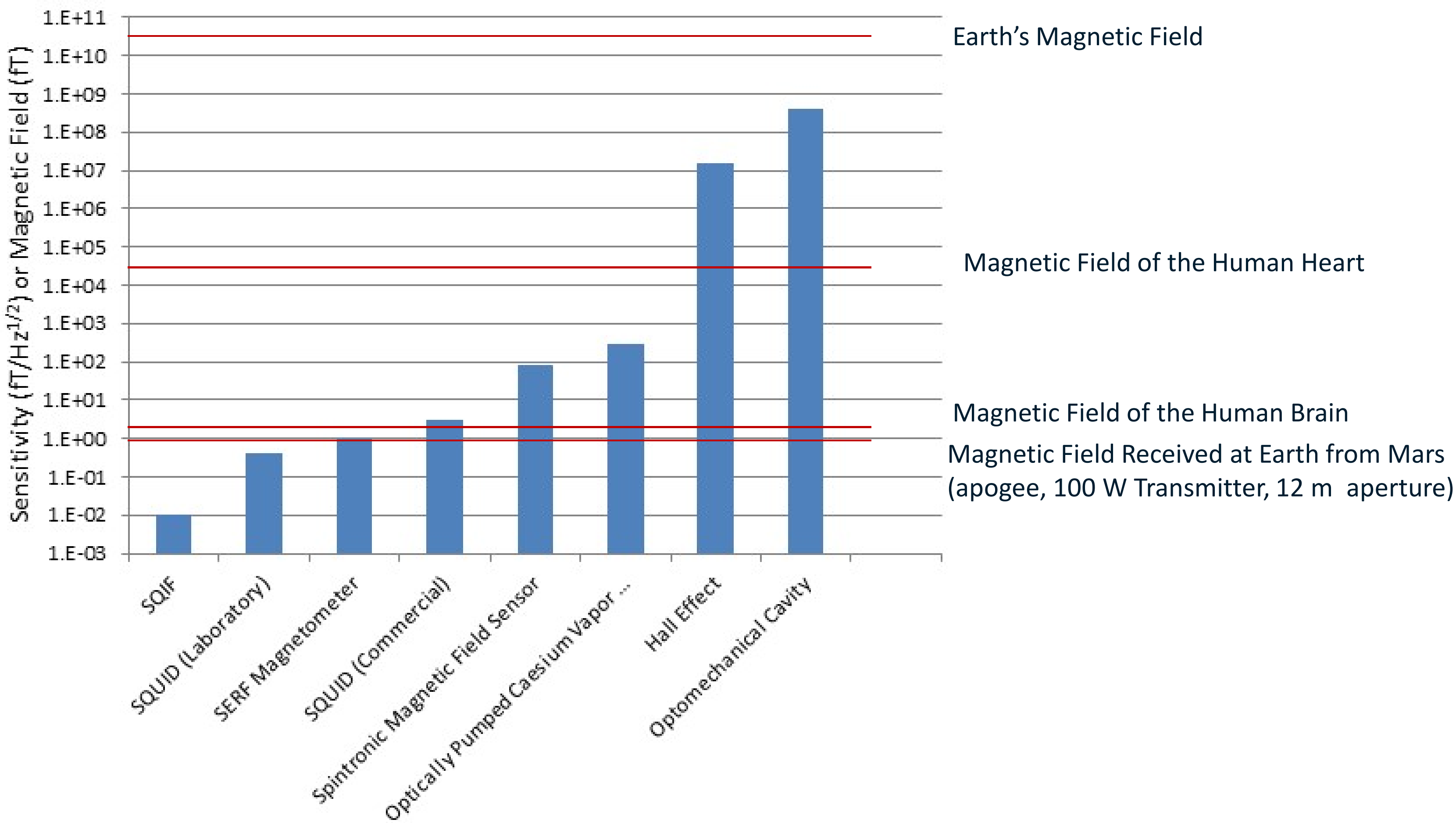

What is Channel Capacity?

- **Capacity**
  - Is the *maximum information rate* that can be achieved across a channel with an arbitrarily small probability of error
  - Represents the *maximum mutual information* between the output (transmitter) and input (receiver) across a channel
  - Units of capacity are *bits per second*
- **Related performance metrics**
  - *Photon Information Efficiency*
    - PIE, bits per photon
  - *Dimensional Information Efficiency*
    - DIE, bits per mode
  - *Spectral Information Efficiency*
    - SIE, bits per second per Hertz

Example: Shannon capacity for Additive White Gaussian Noise (thermal) channel

$$C = B\ \log_2\left(1 + \frac{S}{N}\right)$$

C = capacity (bits / time)
B = bandwidth (1 / time)
S = signal power (energy / time)
N = noise power (energy / time)

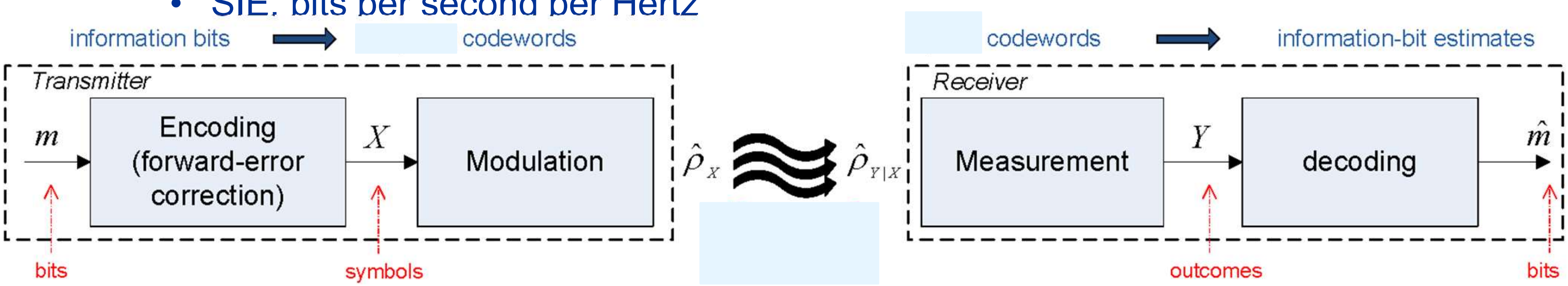

Pulse Position Modulation (PPM)

- **Pulse Position Modulation (PPM, a form of generalized OOK) of a laser transmitter in combination a photon counting receiver is a near-optimal configuration for high PIE**
  - – "Poisson channel" model applies
  - – Trades low DIE for high PIE
  - – Uses high peak-to-average power lasers
  - ✓ **Photon Counting – Direct Detection (PC-DD) is easy to implement**
  - ✓ **Forward Error Correction codes are already known that approach within 1 dB of capacity**

M Alphabet size
T_s Slot Width
T_w Symbol Time
T_G Guard Time

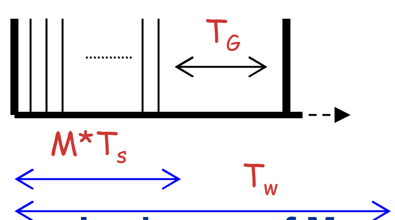

- **In PPM, a single laser pulse in one of M symbol slots encodes $\log_2 M$ information bits**
  - – Additional non-signal slots may be appended to the PPM symbol to allow for slot clock recovery at the receiver and/or pulsed laser reset time

- With no minimum slot width constraint in place, the capacity of the Poisson channel may be bounded as:

$$
\begin{aligned}
C \le C_{\text{ook}} &= \tfrac{1}{\ln 2}\big((\lambda_s + \lambda_b/M)\ln(1+\lambda_b/(M\lambda_s)) + \\
&\quad ((M-1)/M)\lambda_b \ln(\lambda_b/(M\lambda_s)) - \\
&\quad (\lambda_s+\lambda_b)\ln((1+\lambda_b/\lambda_s)/M)\big) \ \text{bits/sec}
\end{aligned}
$$

Where
- λs = mean signal photons/second
- λb = mean noise photons/second

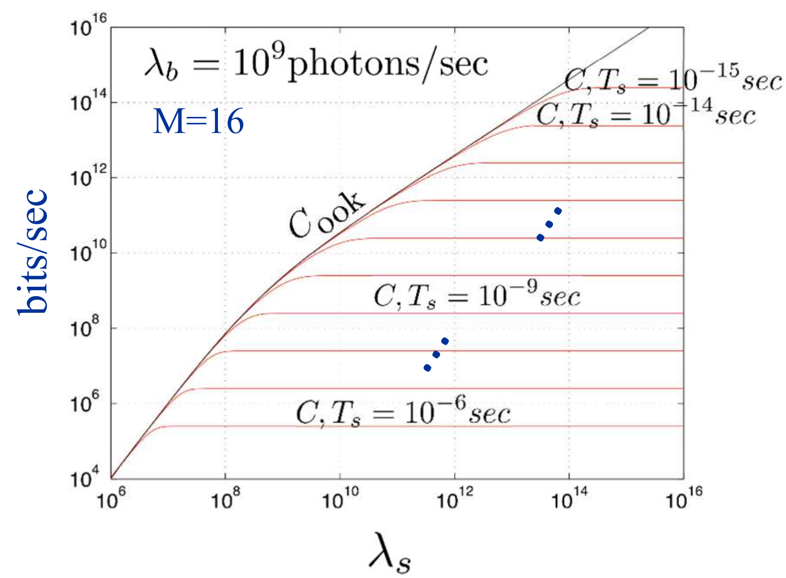

RF / Optical Capacity

- **Although optical outperforms RF at high data rates, RF can outperform optical at large ranges and under high background conditions**

$$C = \frac{4}{\pi}\frac{\alpha_{rf}\eta_{r(rf)}d^2_{r(rf)}}{N_0 R^2}\left[\frac{2\ln M}{M}\frac{I_S\Omega_S\lambda_S R^2}{\alpha_{op}\eta_{r(op)}}\right]^{\frac{\beta_{rf}}{\beta_{op}}}$$

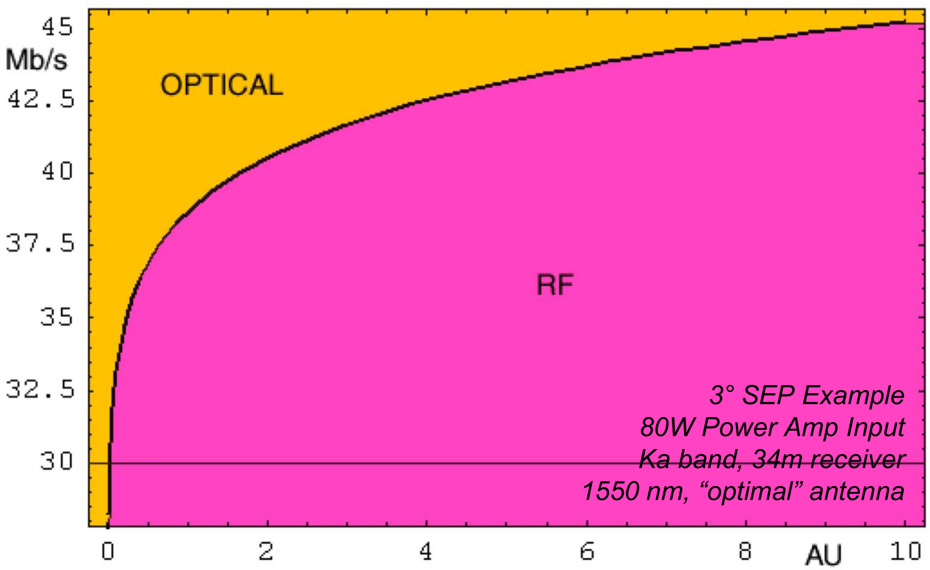

Equal-Mass Equal Capacity RF-Optical Performance

William Farr, Space Optical Communications, Jet Propulsion Laboratory, December 2011

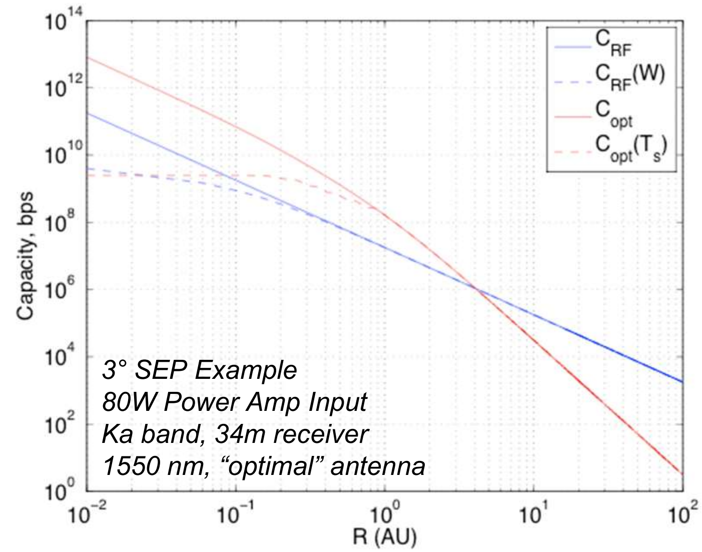

$$C_{RF}(W) = W\log_2\left(1+\frac{P_r}{N_0 W}\right)\ \mathrm{bps}$$

$$\begin{aligned} C_{opt} &= \left((P_r + P_b/M)\log_2(1+MP_r/P_b)\right. \\ &\left. -(P_r+P_b)\log_2(1+P_r/P_b)\right)/E_\lambda\ \mathrm{bps}\end{aligned}$$

For Pr> 2 Pb ln M/M, the capacity goes as $1/R^2$, for Pr< 2 Pb ln M/M the capacity goes as $1/R^4$

Microwave Kinetic Inductance Detectors: Basic Principles

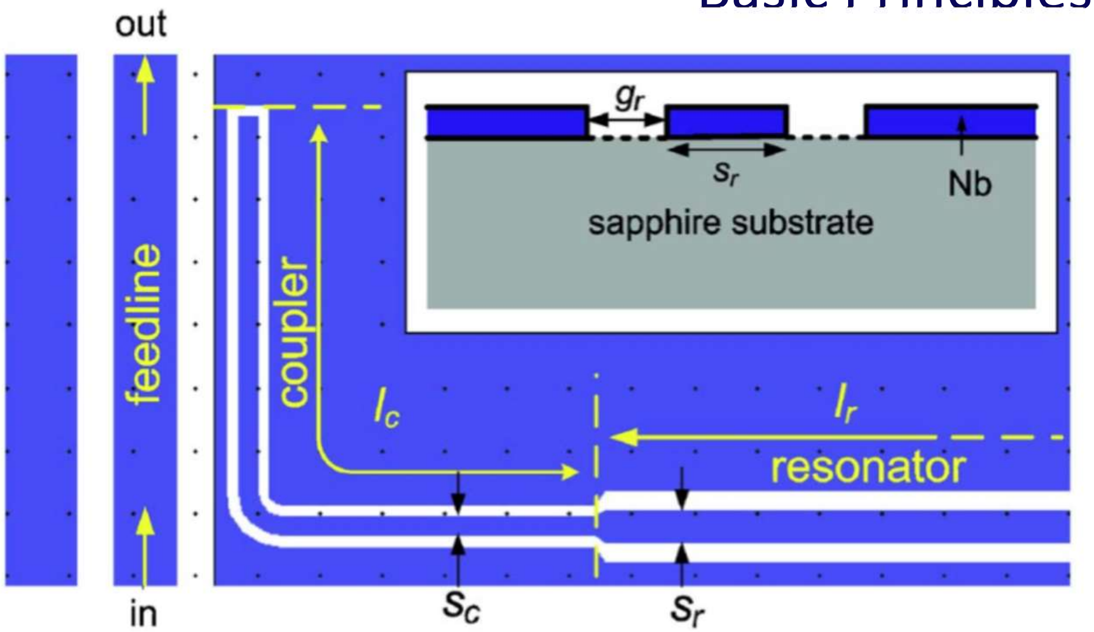

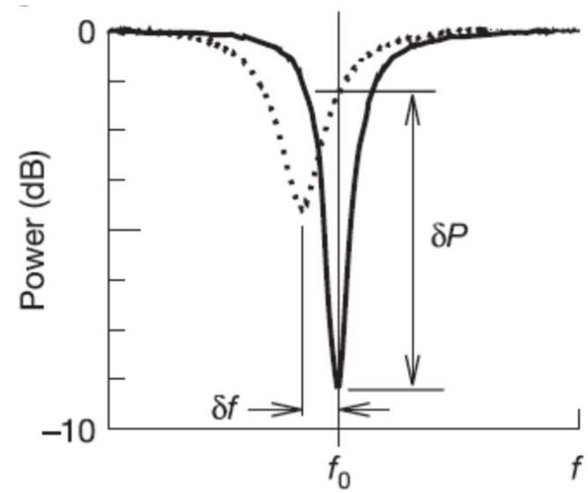

- Resonators gain **kinetic inductance** from Cooper pair motion when $T<T_c$.
- Photon absorption breaks pairs, perturbing the resonance.
- Usually $T<<T_c$ to maximize Cooper Pair population, minimize spontaneous pair breaking

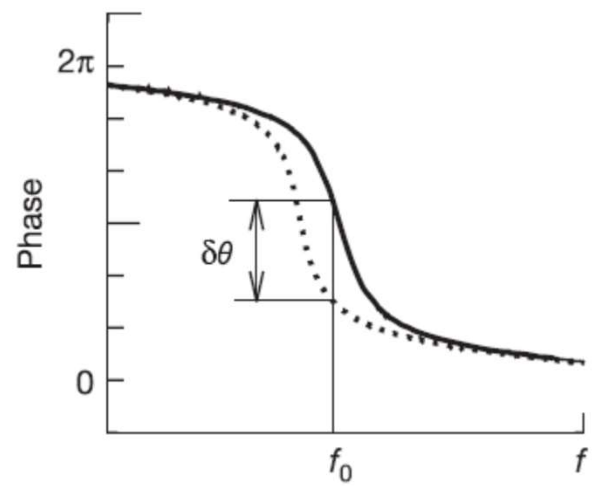

B. Mazin, AIP Conference Proceedings, 1185, 135-142 (2009)

Kinetic Inductance (KID) and Superconducting Nanowire Single Photon Detectors (SPD)

Superconducting Nanowire SPD

- Superconducting nanowire single photon detectors (SPDs) are used where precision timing
- and single photon sensitivity are required
- Films (e.g. NbN) are generally about 10 nm thick and ≈ 200 nm wide
- Devices are biased with a constant current near the critical current such that absorbed photons dissociate Cooper pairs and drive the nanowire normal.
- Generally formed into an array or meandering complex to improve detection efficiency.
- Generally cooled below 100 mK to minimize the quasiparticle population
- Spontaneous pair breaking and recombination is biggest noise source above ~100mK

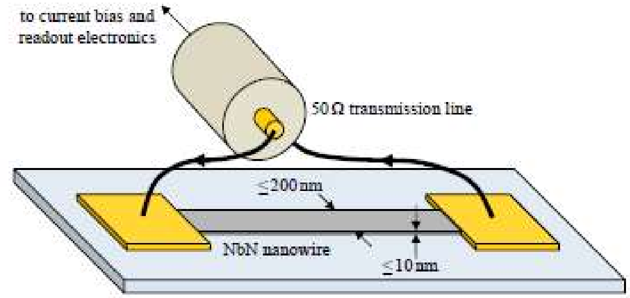

Simplified illustration of superconducting nanowire single photon detector [1]

Kinetic Inductance SPD

- Frequency of a transmission line resonator is inversely proportional to the square root of (geometric + kinetic) inductance
- Shift in the density of quasiparticles due to radiation results in a change of the kinetic inductance
- Sensitivity proportional to Q
- Noise equivalent power determined by quasiparticle generation–recombination can be as small as 10^{-19} W/√Hz using He_3 cryostats
- Primary application of these devices has been astronomical observations

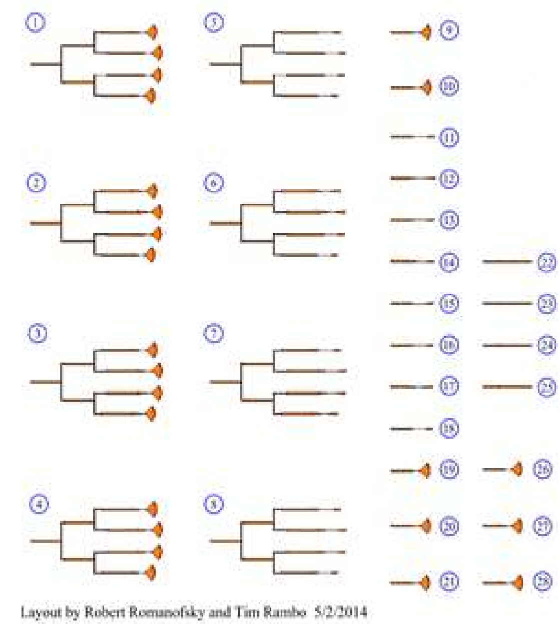

Layout of prototype kinetic inductance SPD tapered resonators

GRC: Design and fabricate KIDs, investigate response near and at ~1/3 Tc

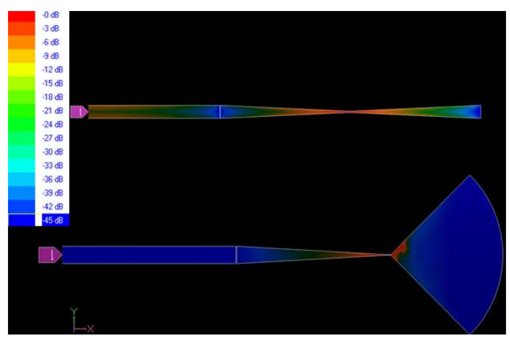

Modeled current distribution X-band resonator

[1] Multi-element Superconducting Nanowire Single Photon Detectors, E. Dauler, PhD Dissertation, 2009

SNSPD Operation and Assembly

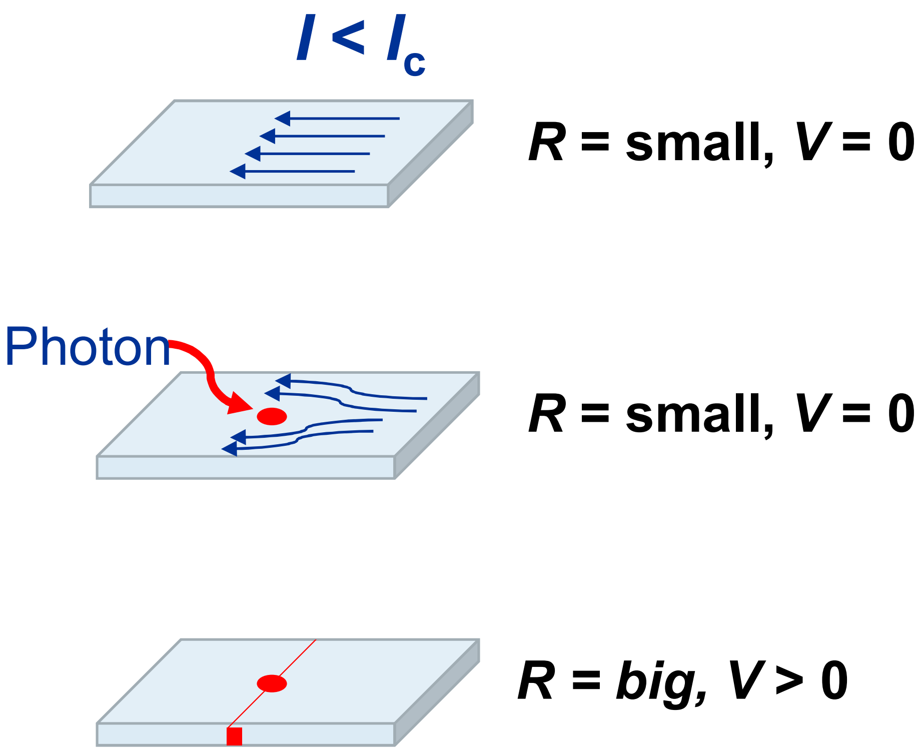

Standard operating temp ≤ 2.5 K

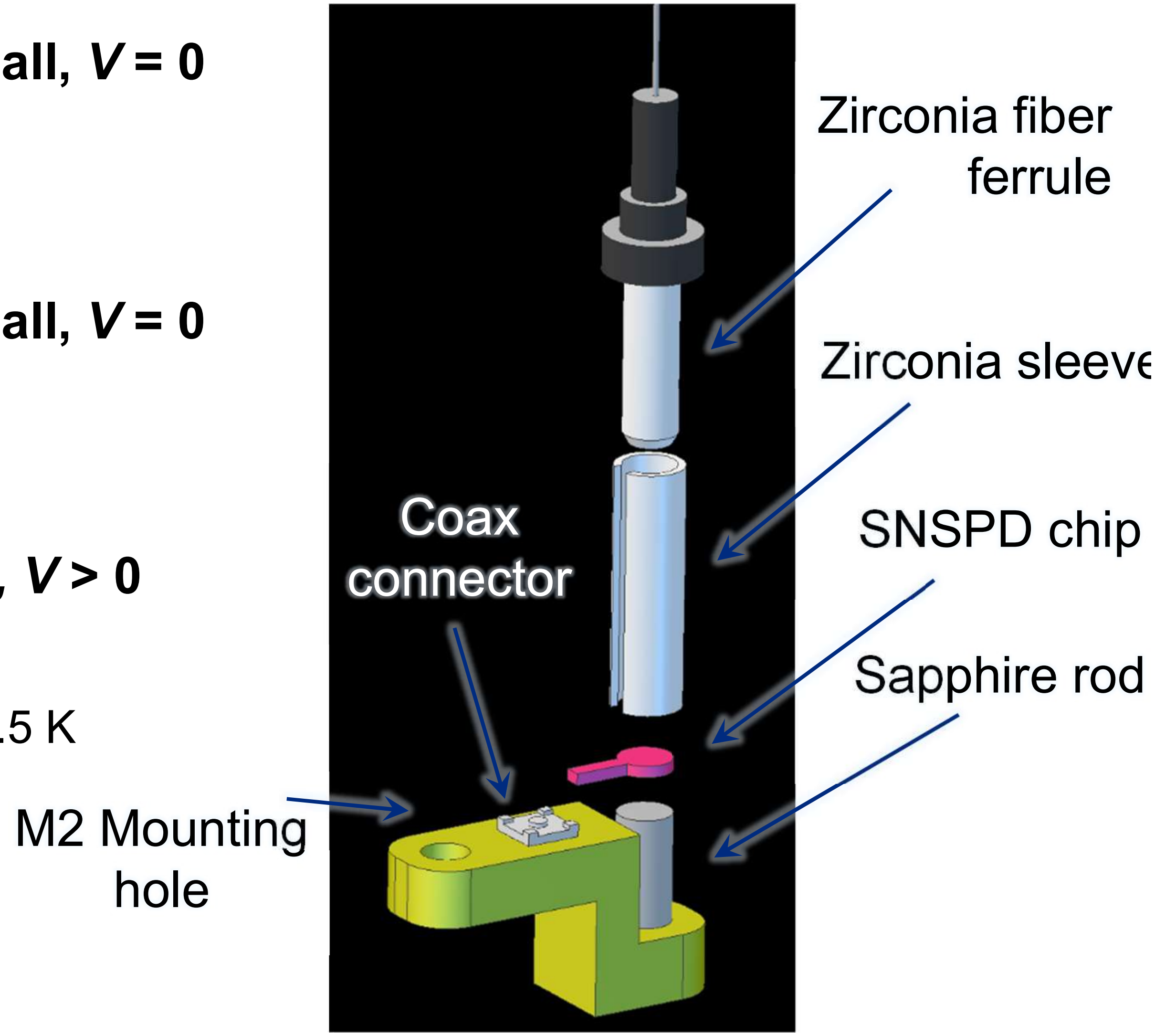

Courtesy of www.QuantumOpus.com

SNSP Detectors

- Single-photon detectors at near-infrared wavelengths with high system detection efficiency (>80%), low dark count rate (<1 c.p.s.), low timing jitter (<100 ps) and short reset time (<100 ns) are required
- Commercially available turnkey superconducting nanowire single photon detector systems are available now that can support 8 channels (e.g. PhotonSpot, Quantum Opus)

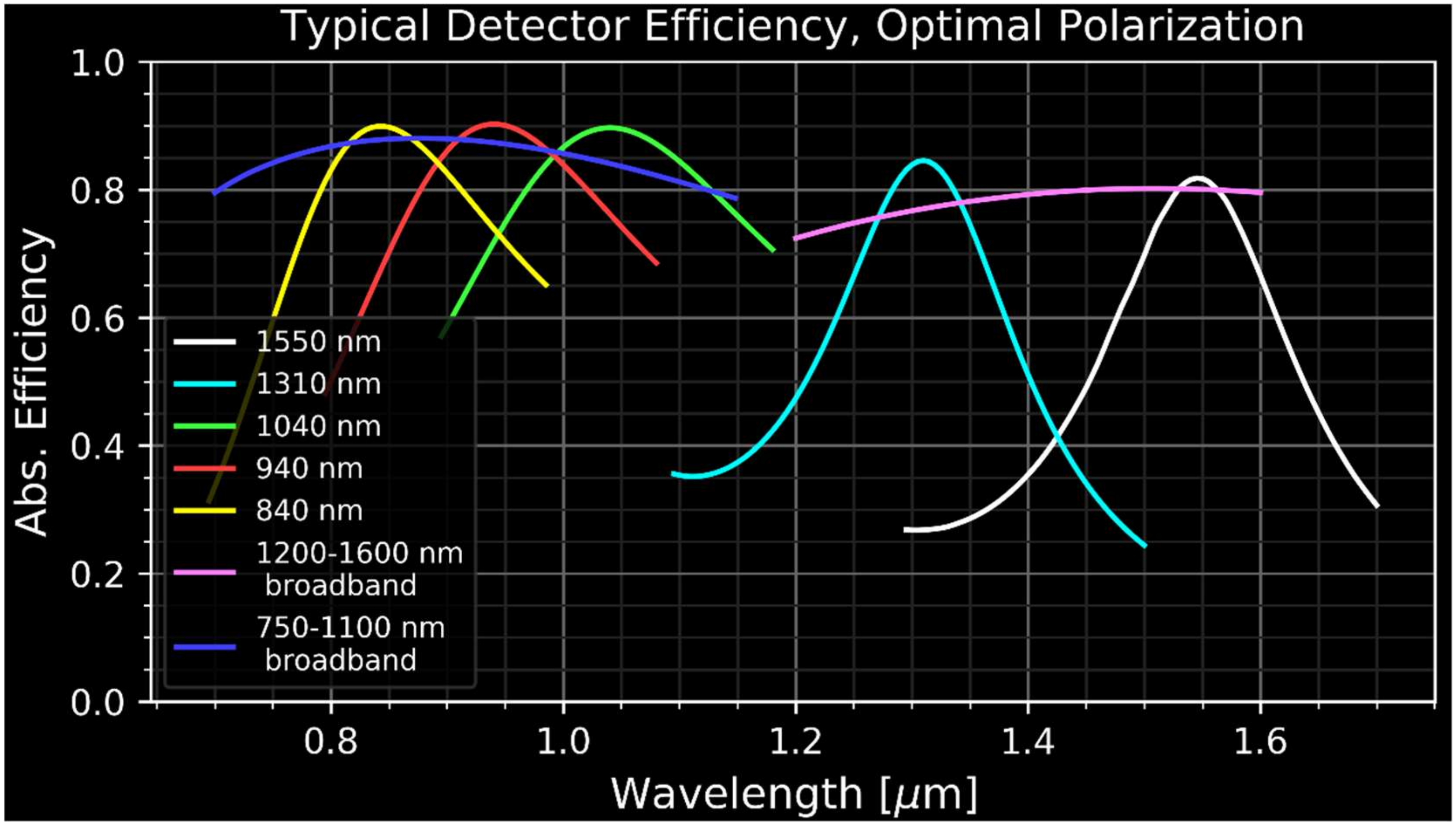

http://www.quantumopus.com/

Subtle Aspects of Coupled Resonators

In a microstrip or coplanar transmission line resonator, the coupling is accomplished by using a narrow (<<λ_g) gap. This discontinuity can be modeled by a capacitive π network, or equivalently, by an ideal transformer. The effect of loading is to increase the conductance of the resonator by an amount equal to the transmission-line characteristic admittance multiplied by the transformer turns ratio ***n.*** Hence, the modified *Q* will be smaller and is given by

$$Q_L = \frac{\omega C_0}{G_0 + n^2 Y_0}$$

It is assumed that the coupled susceptance is negligible compared with the resonator susceptance. A comparison of Q_L with Q_O yields

$$\frac{1}{Q_L} = \frac{1}{Q_0} + \frac{n^2 Y_0/G_0}{Q_0}$$

where n^2Y_o/G_o is the ratio of coupled conductance to resonator conductance and is referred to as the coupling coefficient ***κ.*** The unloaded quality factor may therefore be expressed as:

$$Q_0 = (1 + \kappa)Q_L$$

When *κ* < 1, the resonator is under-coupled and is defined by:

$$\kappa = \frac{1 - |\Gamma_{io}|}{1 + |\Gamma_{io}|} \equiv \mathrm{VSWR}^{-1}$$

When *κ* > 1, the resonator is over-coupled and is defined by:

$$\kappa = \frac{1 + |\Gamma_{io}|}{1 - |\Gamma_{io}|} \equiv \mathrm{VSWR}$$

Subtle Aspects of Coupled Resonators

The degree of coupling can therefore be determined from an inspection of the Smith chart impedance plot. The three possibilities correspond to d = 1 (critically coupled), d < 1 (under-coupled), and d > 1 (over-coupled)

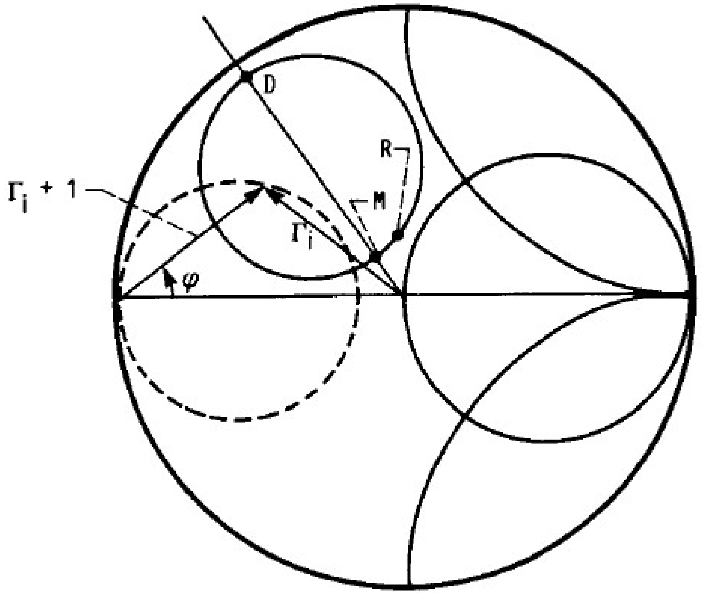

Ideal impedance locus for under-coupled resonator (dashed line) and translated locus in presence of coupling loss and reactance. Point *D,* detuned resonator; point R, unloaded resonant frequency; point *M,* loaded resonant frequency; Γ_i, input reflection coefficient.

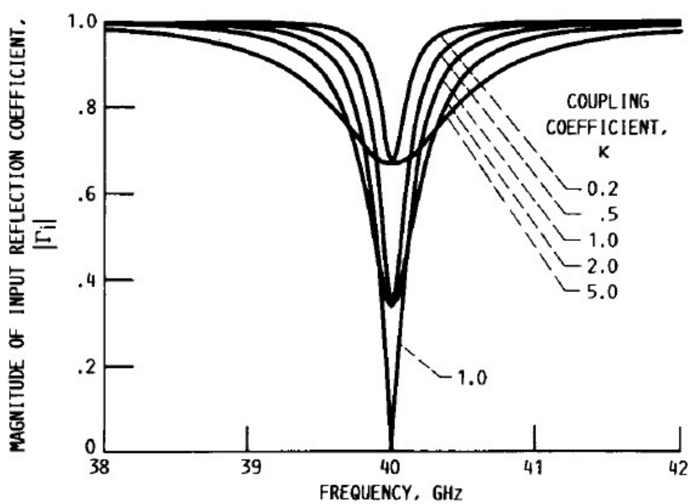

Typical resonator reflection coefficient magnitude with various degrees of coupling for Q_o = 100 in absence of series loss.

Subtle Aspects of Coupled Resonators

The apparent resonant frequency of an inductively or capacitively coupled resonator is pulled from the natural resonant frequency of the isolated circuit because of the reactance or susceptance associated with the coupling mechanism.

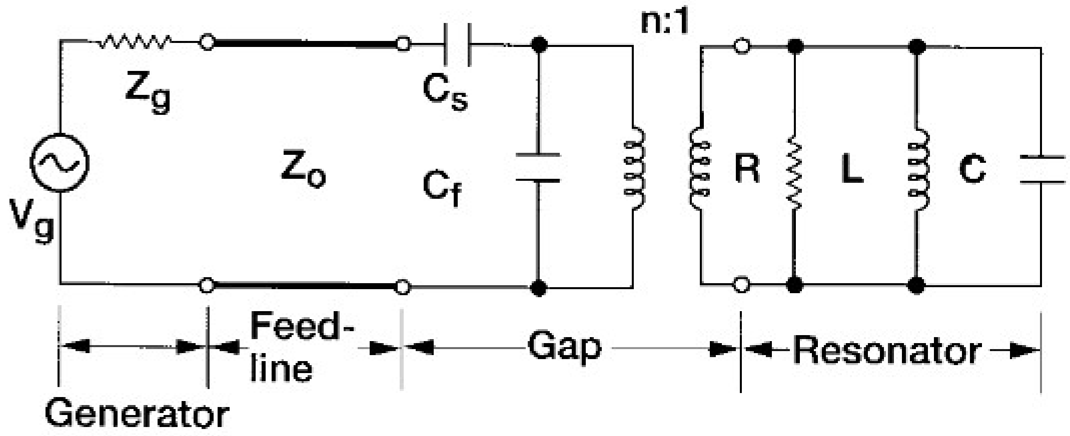

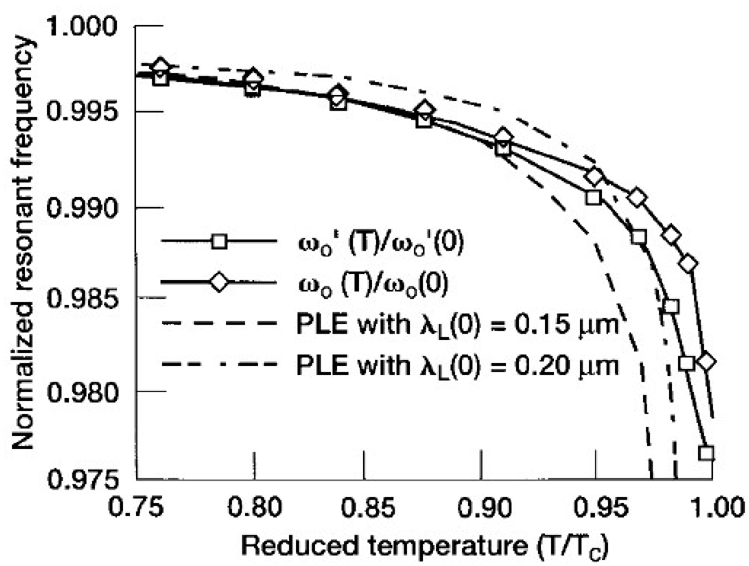

Semiconductor Receiver versus SQIF Receiver (*E* vs. *B*)

SQUIDs can detect magnetic fields lower than one flux quantum $h/(2e) \approx 10^{-15}$ Wb, 10^{-18} Wb reported in the literature (DC)

Conventional Receiver

Mars link at 64 MBPS

- EIRP = 84 dBW ($\approx 2.5 \times 10^{8}$ W)
  - Assumes 100 W TWT, 12 m aperture
  - Range=3.7×10^{8} km
- Power density at receiver $\approx 2.8 \times 10^{-16}$ W/m^2
  - Electric Field $\approx 4.6 \times 10^{-7}$ V/m
  - Displacement flux density $\approx 10^{-18}$ C/m^2
- Receive Antenna Aperture
  - QPSK, Block Turbo Code, 3 dB margin
  - Required E_b/N_o=4.6 dB

Aperture size 34 meters

SQIF Superconducting Receiver

Mars link at 64 MBPS

- EIRP = 84 dBW ($\approx 2.5 \times 10^{8}$ W)
  - Assumes 100 W TWT, 12 m aperture
  - Range=3.7×10^{8} km
- Power density at receiver $\approx 2.8 \times 10^{-16}$ W/m^2
  - Electric Field $\approx 4.6 \times 10^{-7}$ V/m
  - Displacement flux density $\approx 10^{-18}$ C/m^2
  - Magnetic Field $\approx 10^{-9}$ A/m
  - Magnetic flux density $\approx 10^{-15}$ Wb/m^2
- Receive Antenna Aperture
  - Flux Concentrator
  - Mechanical refrigerator at 4K

Aperture Size ???

Can We Make a "Noiseless" Receiver

The fundamental argument against a noiseless receiver goes something like this. From the uncertainty principle $\Delta E \Delta t = h/(4\pi)$ where energy $E=hf$, h is Planck's constant, f is frequency and t is time. (The more localized energy is in frequency, the less it is localized in time.) Since $\Delta\theta = 2\pi f \Delta t$ and substituting $\Delta E = hf\Delta n$ where Δn is photon number uncertainty we conclude:

$$\Delta n \, \Delta\theta \geq 1/2 \qquad (1)$$

Hence a large number of photons must be received if the phase is to be known accurately. A noiseless amplifier would produce G output photons for every input photon where G is the amplifier gain (i.e. n_i input photons produce $n_o = Gn_i$ output photons). For a linear amplifier, the output phase θ_o is equal to the input phase θ_i plus some constant. A perfect detector would permit the measurement of n_o and θ_o with an uncertainty $\Delta n_o \, \Delta\theta_o = ½$. But uncertainty Δn_o corresponds to an input uncertainty $\Delta n_i = \Delta n_o/G$ and output uncertainty $\Delta\theta_o$ corresponds to input uncertainty $\Delta\theta_i = \Delta\theta_o$. Therefore the apparent measurement uncertainty is $\Delta n_i \, \Delta\theta_i = 1/(2G)$ in violation of equation (1) leading to the conclusion that a noiseless amplifier is impossible.

Nevertheless, with a sufficient number of SQIF loops, T_e will approach and possibly reach the quantum limit hf/k, where k is Boltzmann's constant.

Receiver Technology @ 32 GHz	Sky Noise Temperature (K)	Receiver Noise Temperature (K)	System Noise Temperature (K)	Sensitivity Improvement over MASER (dB)	Sensitivity Improvement over 20 K HEMT (dB)
MASER	10	9.0	19.3	-----	+1.5
HEMT	10	16.1	27.0	-1.4	-----
SQIF	10	1.5	11.6	+2.3	+3.6

Superconducting Quantum Interference Filter (SQIF) – potentially the world's most sensitive microwave receiver (in fact, a "noiseless" receiver!)

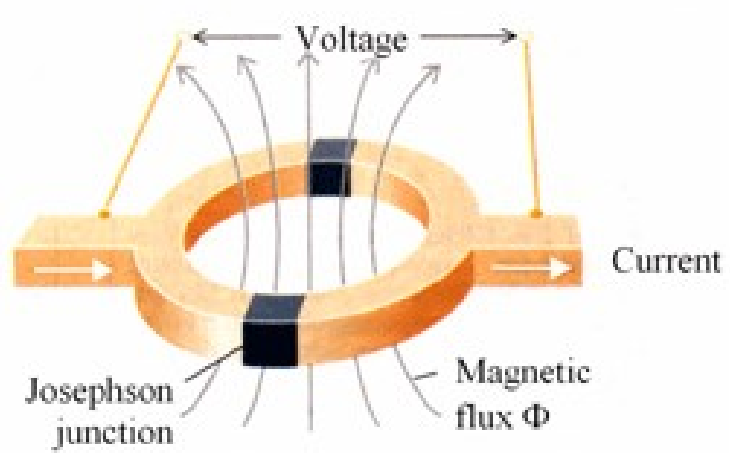

When a SQUID[1] (the building block of a (SQIF) is biased with a constant current, the voltage across it oscillates with increasing ϕ and period ϕ_o (h/2e). SQUIDs can detect magnetic fields lower than one flux quantum, with 10^{-18} Wb reported in the literature. Φ is the magnetic flux from the communications signal that pierces the superconducting loop

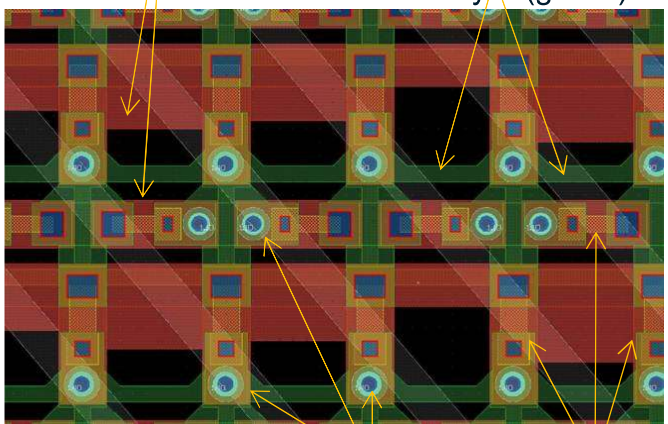

A SQUID consists of a superconducting loop bifurcated by two Josephson junctions (superconducting-insulator-superconducting sandwiches). A SQIF is an array of N individual SQUIDs – with incommensurate loop area. In this case, as N becomes larger the signal-to-noise ratio increases as $N^{1/2}$ and the noise diminishes to zero for very large N (i.e. an ideal receiver!)

[1] J. Clarke, Scientific American, August, 1994

Rationale for Pursuing SQIF Technology Goals and Requirements

SQIF: A potentially "noiseless" receiver

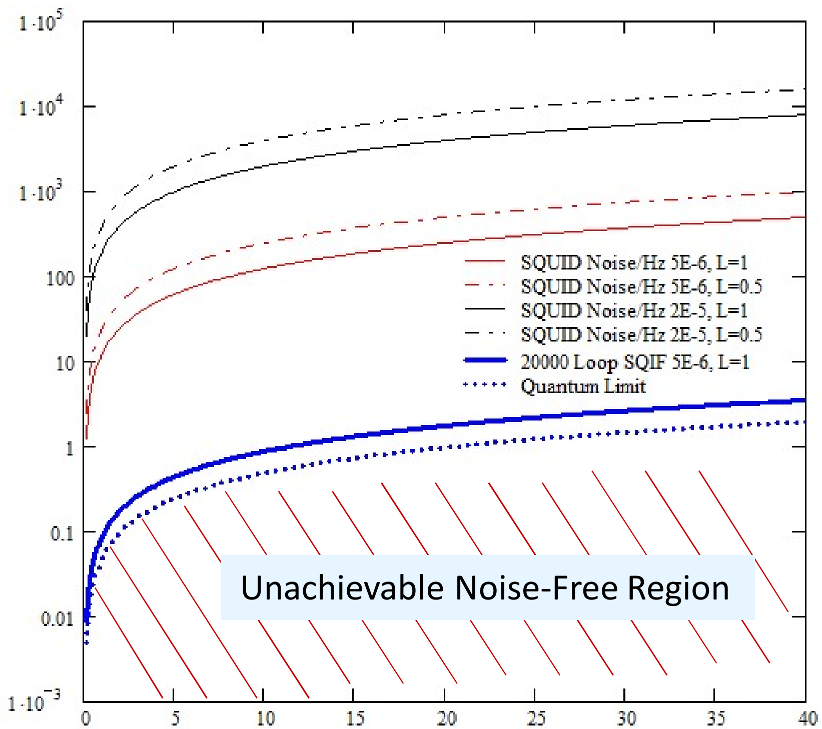

Calculated SQUID and SQIF sensitivity (noise temperature) as a function of frequency with loop inductance as a parameter.

- The calculation assumes flux noise spectral density ($\phi_o/\sqrt{Hz}$) stays white to the frequency range of interest which should be valid as long as we stay well below the Josephson frequency.
- A noise spectral density of $5x10^{-6}$ is typical for a Nb SQUID.
- A SQIF with N=20,000 loops (solid blue curve) comes very close to the quantum limit.
- The analysis additionally assumes the noise indeed continues to scale inversely as $N^{½}$. In practice the magnetic field must be efficiently directed through the array plane.

Superconducting Quantum Interference Filter (SQIF)

Operating Principles

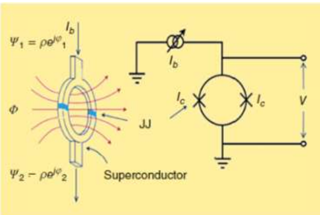

A single SQUID

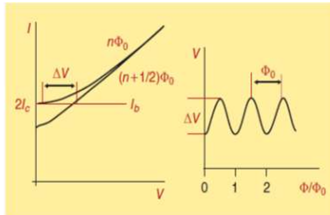

Periodic flux-to-voltage response

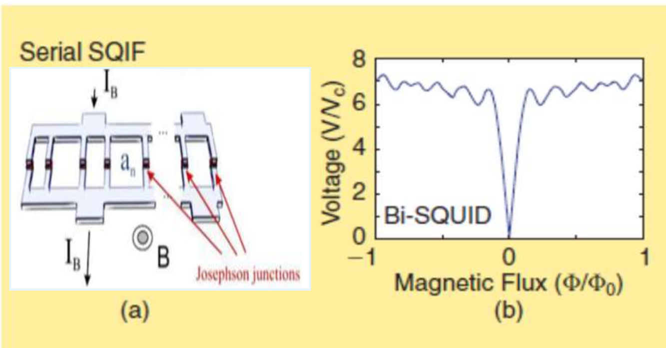

- SQUID voltage response is periodic in the applied magnetic field
- SQIF is an array of SQUIDs of incommensurate area with a unique magnetic flux-to-voltage response
- Sensitivity improves with arraying more SQUID cells ($S/N \sim \sqrt{N}$)

Integrated circuit of 2-D SQIF arrays

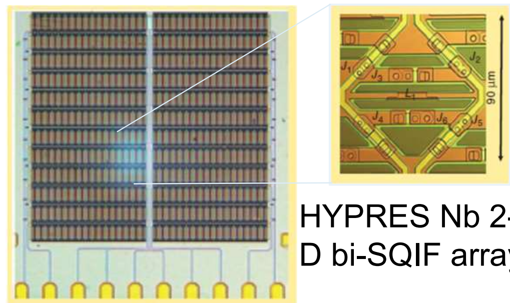

HYPRES Nb 2-D bi-SQIF array

Comparative Technologies

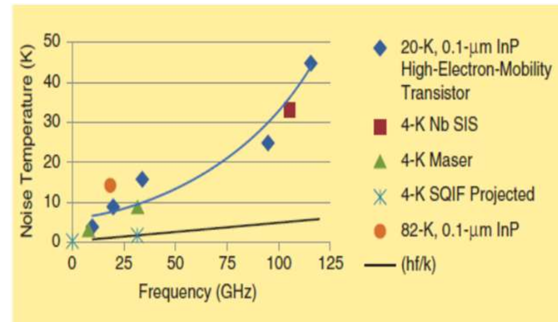

SQIF receiver conceptual block diagram

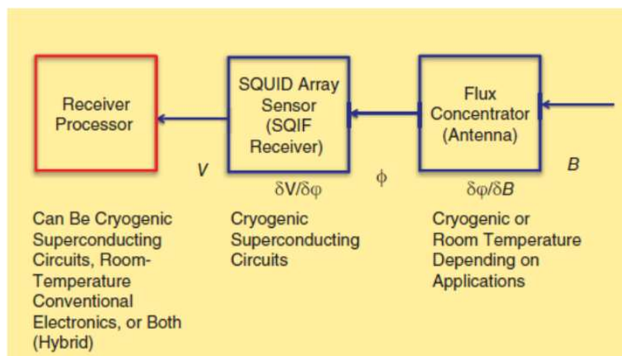

- Receiver will consist of a flux concentrator (antenna), SQIF sensor, and digital signal processor

- Energy sensitivity of about 10^{-31} J/Hz, compared to semiconductor 10^{-22} J
- Sensitivity approaches quantum limit, while increasing dynamic range and linearity
- Attractive for wideband-sensitive receivers
- Robust to variation in fabrication spread (e.g. junction critical current, inductance, etc.)

SQIF Testing

Typical Measured Voltage Flux Response

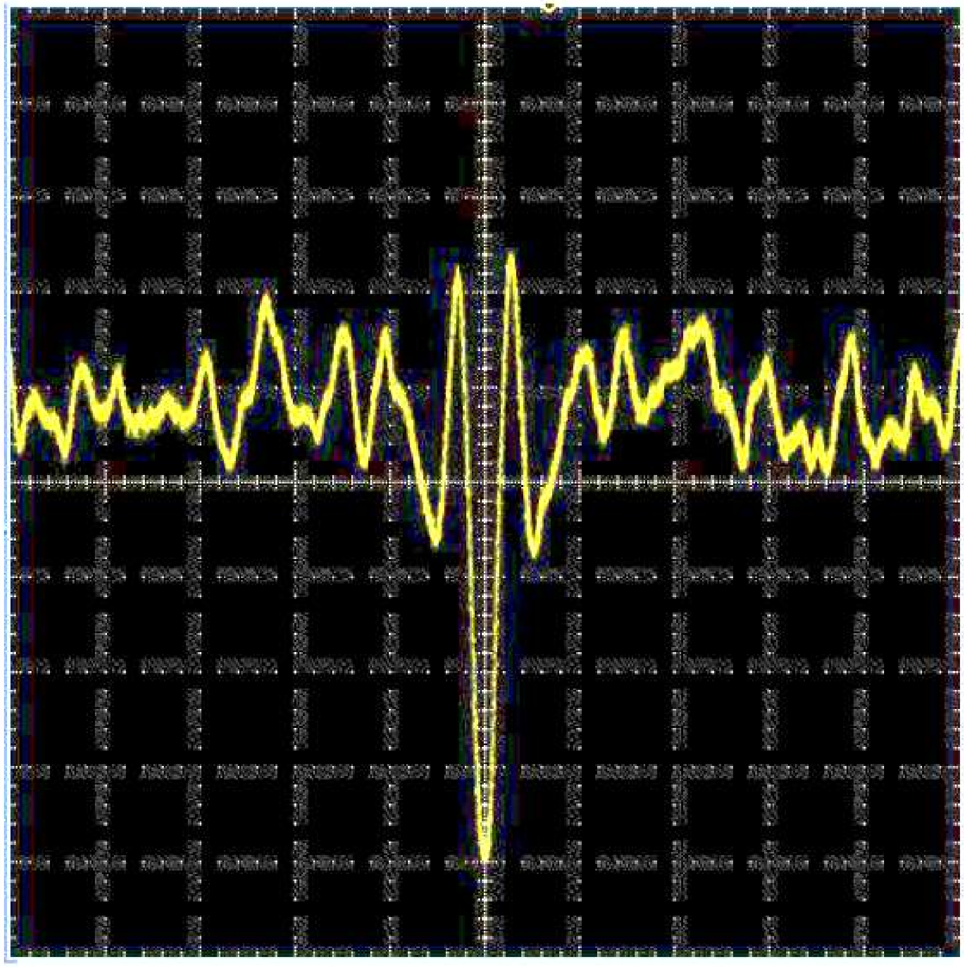

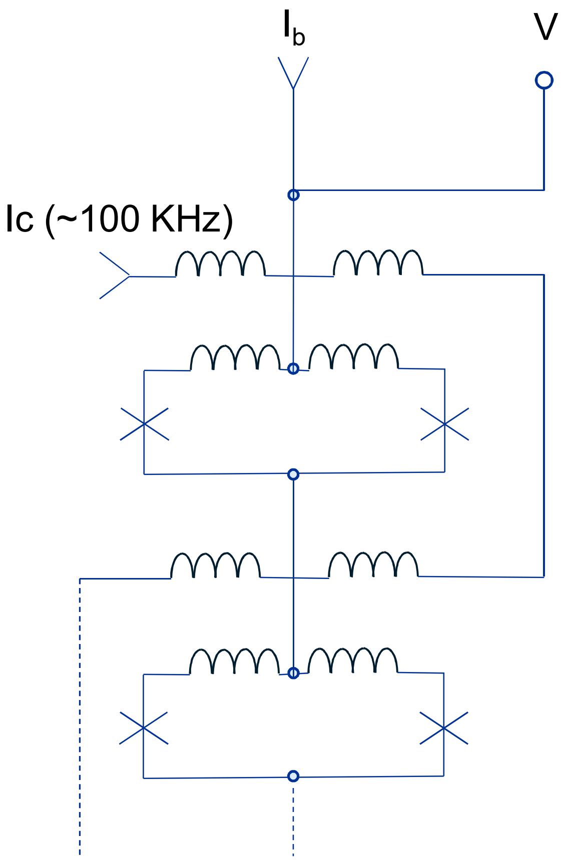

Measurements start by verifying Flux-Voltage transfer Characteristic. Operating point is selected mid-point of anti-peak slope (I_c and I_b) 50 µV/div, 2 mA/div

Results

First reported high gain results at X-band, September 2014

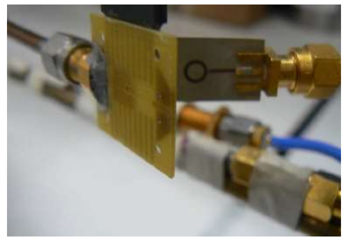

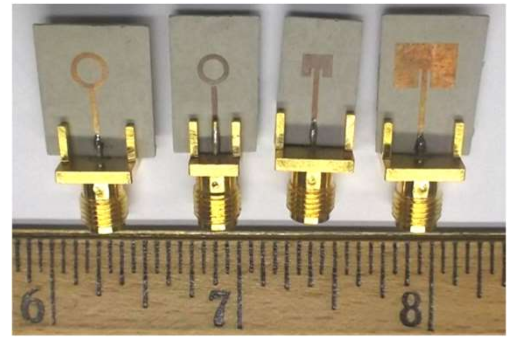

X-band test antennas

Focused Issue Featured Article: *Quantum Sensitivity: Superconducting Quantum Interference Filter-Based Microwave Receivers*

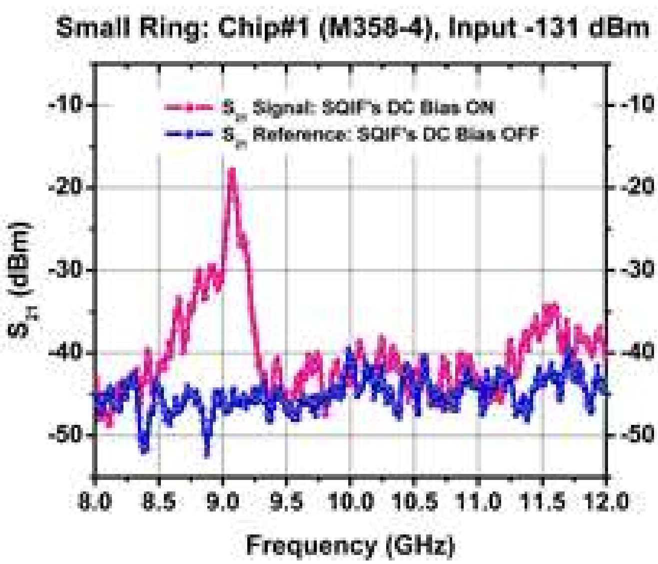

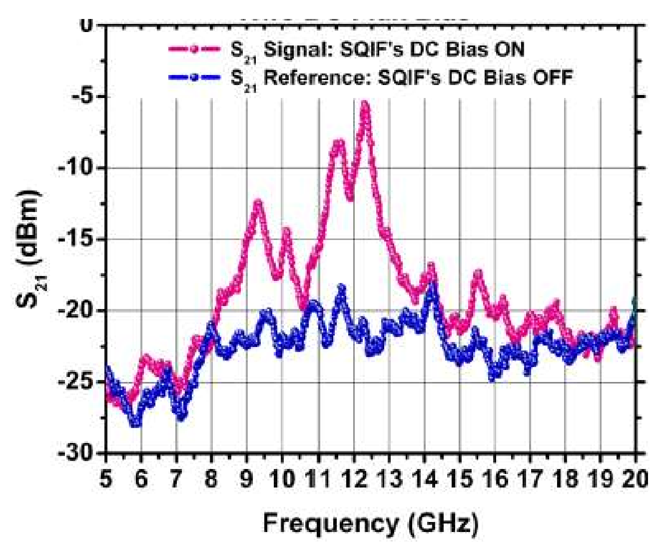

Voltage response of the SQIF array in the ON and OFF states

April, 2017: Four representatives from CSIRO visit GRC to conduct tests on unique high temperature superconductor SQIF devices fabricated by CSIRO.

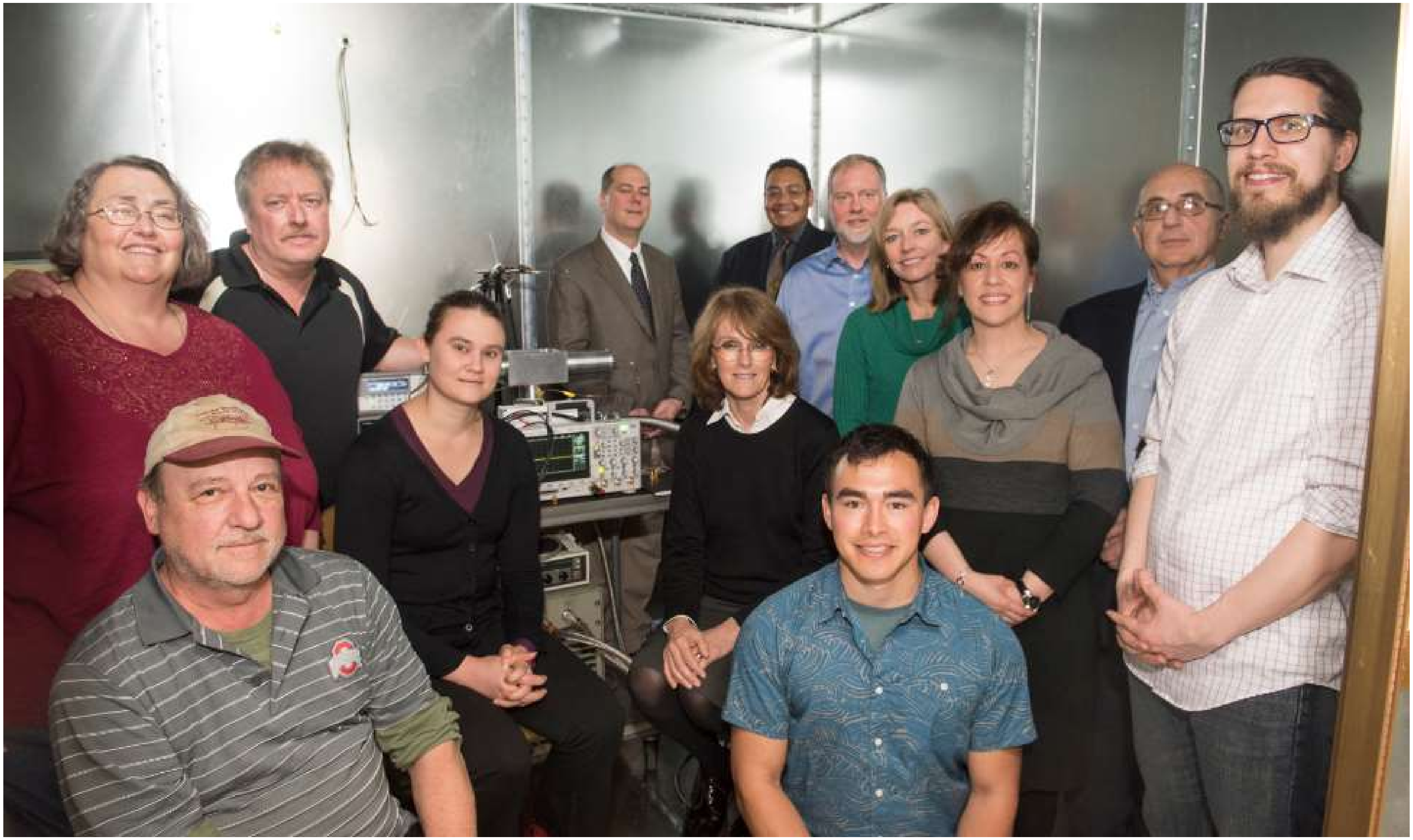

The unique voltage response of SQIF-sensors is intrinsically robust against scatter of junction parameters in the array (self averaging)

An Optical Ground Array: Introduction

- The purpose of this study is to outline the design of an optimal array of optical telescopes to emulate performance of a monolithic 12 m telescope in support of deep-space communications. In this case, optimal means minimizing the initial capital investment and operational cost while maintaining performance requirements of the deep-space link. The design is approached from a practical, engineering perspective. Pulse position modulation (PPM) signal formatting and photon counting detectors are assumed at each telescope in the array. That is, the telescopes function as so-called light buckets, so direct detection (as opposed to coherent reception) of the received signals is assumed, and there is no intention to consider active compensation for atmospheric turbulence-induced phase fluctuations.

- The projected cost of a 12 m diameter monolithic optical receiver system is ≈$120 M. It will be shown that given certain assumptions the optical array cost is close to 2/3 this estimate.

- A parametric analysis among aperture size, detector size, and primary mirror surface quality, in the context of field-of-view expansion, is presented to minimize the cost function.

- Besides potentially very substantial cost savings, other advantages of a telescope array include: minimal gravitational effects (i.e. primary mirror/sub-reflector structural sag), reliability through redundancy, and scalability. A possible drawback of a large telescope array is the complexity associated with synchronization of the individual telescope PPM signals.

- From empirical data

$$C = q\,(\alpha\,(D/\sqrt{q})^{x} + 0.47q^{-0.33}) \qquad (1)$$

where C is the cost in millions of dollars, D is the telescope diameter in meters, q is quantity, and x is ≈ 2.6. The value of α is a function of “blur circle diameter” which is essentially corresponds to resolution in arcseconds. Each telescope has an independent focal plane detector, and that detector is cooled with a closed cycled helium refrigerator. The term on the right represents refrigerator cost.

Array Cost Minimization (Aperture vs. Quantity)

Estimated telescope array cost as a function of the number of telescopes to emulate a single monolithic 15 m (red), 12 m (blue) and 10 m (black) monolithic telescope. In all cases an alpha=0.2 is assumed (this corresponds to a 0.5 arcsecond spot size).

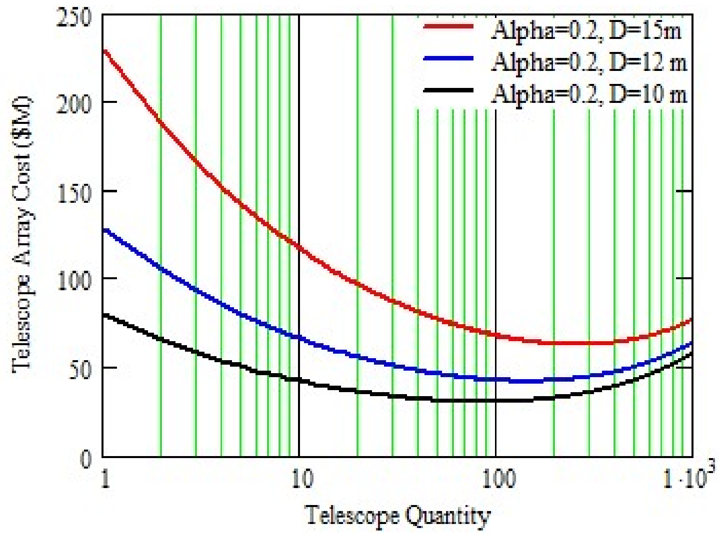

Corresponding array telescope diameter (m) to emulate equivalent monolithic reflector as a function of telescope quantity for the three different monolithic telescope cases.

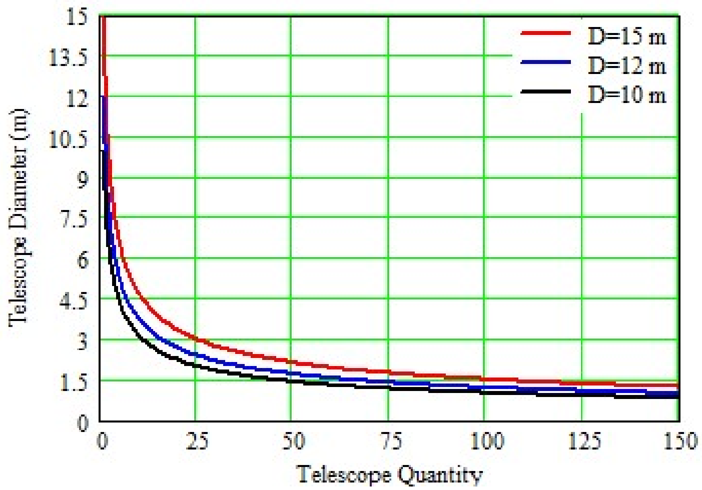

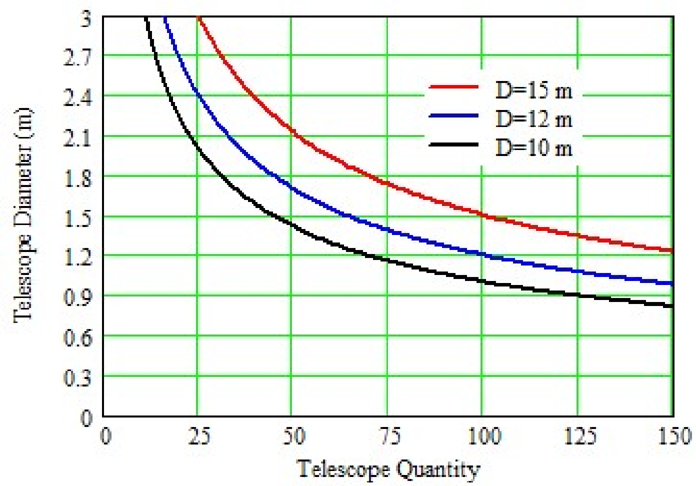

Life Cycle Costs and Dome Costs

Estimated life-cycle cost, in today's dollars, of a monolithic 12 m aperture telescope and a 141 element array of 1.3 m telescopes accounting for periodic refrigerator replacement.

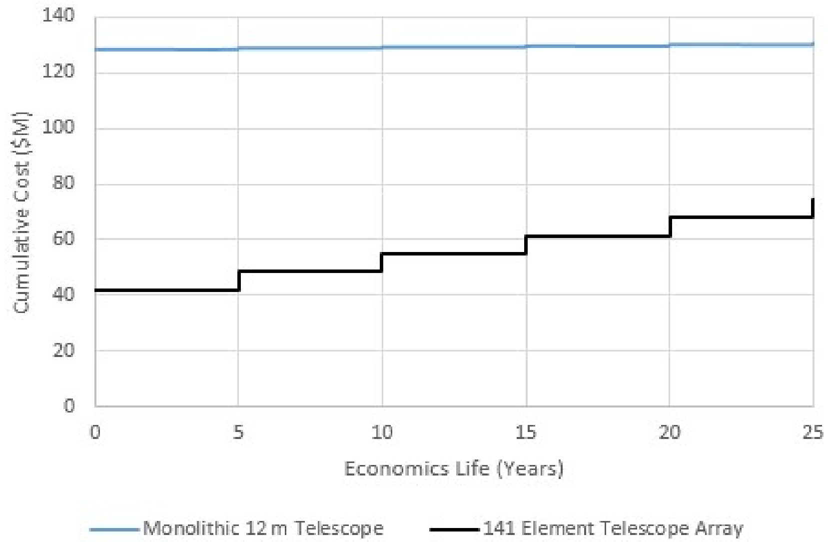

Estimated cost of telescope enclosure based on commercial grade domes

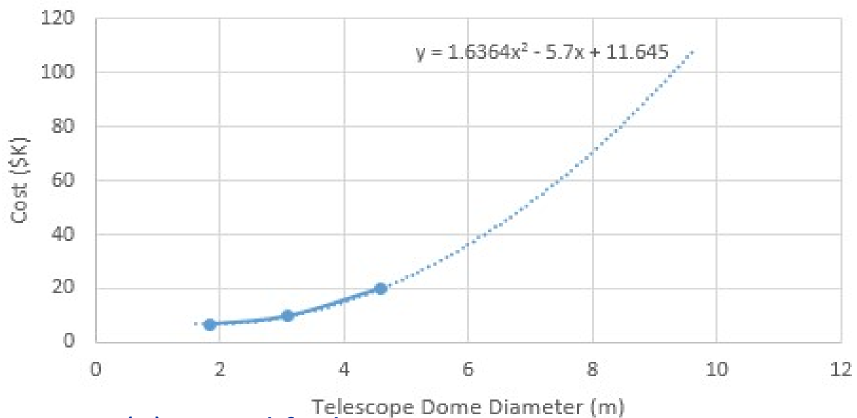

Including telescope housing cost equation (1) is modified as:

$$C \approx q\,(\alpha\,(D/\sqrt{q})^{x} + 0.47q^{-0.33} + 0.02D(D-1) + 0.01) \qquad (2)$$

Atmospheric Turbulence and Detector Size Considerations

- Atmospheric turbulence can cause the actual FoV (i.e. telescope beam solid angle) to be many times the theoretical diffraction limit – essentially increasing background stray light (e.g. scattered sun light). The actual spot size or blur circle diameter is greater than the diffraction limited focus because the turbulence induces angle-of-arrival fluctuations causing spot displacement.

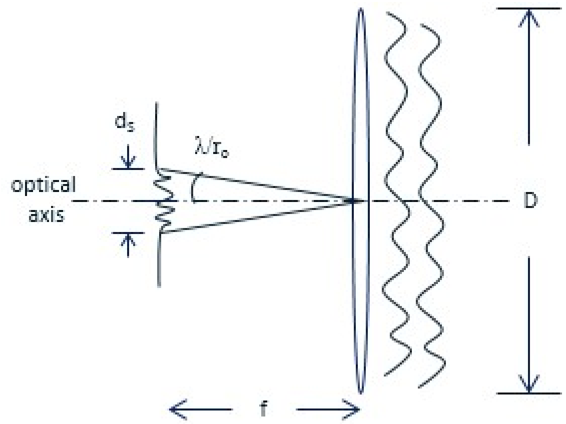

Geometry of basic telescope system illustrating effect of turbulence on point spread function. Turbulence is regarded as distributing the signal into $(D/r_o)^2$ random spatial modes at the detector plane

- The focused spot size becomes $d_S \approx 2\, f\, \lambda/r_o$. A larger detector is necessary to encircle the signal energy, which increases the FoV. Since d_S must be smaller than the detector diameter d_A, this implies

$$f \leq d_A\, r_o/(2\lambda) \qquad (3)$$

- From a manufacturing point of view, an f# >1 is desirable. This leads to the conclusion

$$D \leq f \leq d_A\, r_o/(2\lambda) \qquad (4)$$

- This is on the cusp for a 1.3 m telescope assuming a typical 20 cm Fried parameter.

Mirror Surface Quality Effects and Encircled Energy

- For photometric measurements, the encircled energy is used to represent the integrated flux contained within the detector radius.
- A “real” optical surface has random surface errors which result in scattering and modification of the point spread function.
- The mirror is assumed to contain normally distributed surface errors having zero mean and standard deviation σ (i.e. σ is the RMS roughness in terms of λ.
- The scattered field also depends on the surface autocorrelation function and the characteristic correlation length τ – also assumed to be normally distributed

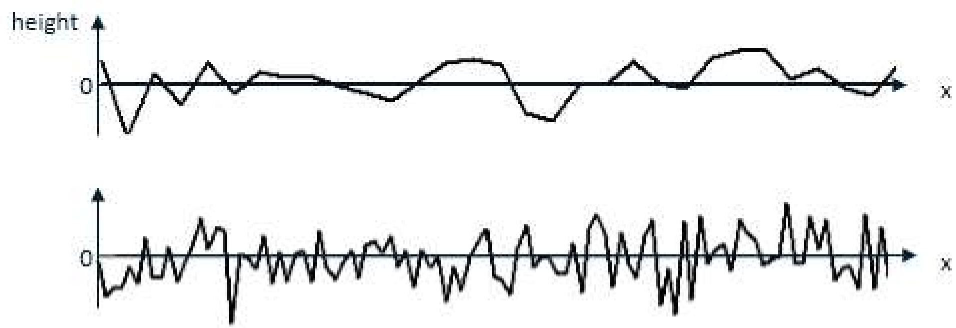

Two different rough surfaces with zero mean and the same RMS value (σ=1) but different correlation lengths.

- The fraction of optical energy, P_E, focused onto the detector is determined by integrating the modified point spread function over the detector area. It is assumed that point spread function is centered on the detector array.

$$P_E = 1 - e^{-(4\cdot\pi\cdot\sigma)^2}\cdot\sum_{m=1}^{\infty}\frac{(4\cdot\pi\cdot\sigma)^{2\cdot m}}{m!}\cdot e^{-\left(\frac{1}{m}\right)\cdot\left(\pi\cdot\frac{\tau}{2}\right)^2} \qquad (5)$$

Scaling Aperture Size to Compensate for Surface Defects

- tradeoff between scaled primary mirror size and RMS surface roughness with correlation length as a parameter

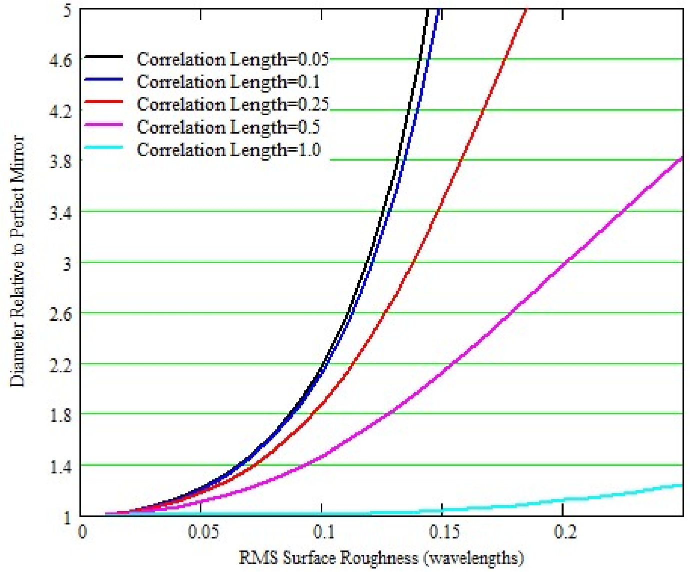

Manufacturable telescope scale factor relative to a perfect mirror as a function of RMS surface roughness, with correlation length expressed in terms of λ/FoV (i.e.≈ $\lambda f/d_A$) as a parameter, and RMS surface roughness ranging up to ¼ λ.

- According to the formulation, for long correlation length (τ>1) there is virtually no mirror diameter increase necessary for surfaces with up to a λ/10 RMS error. For relatively smooth surfaces (say σ/λ<0.1), the diameter scaling is essentially independent of correlation length for τ<0.1 λ/FoV

Hypothetical Mirror Manufacturing Costs

- As a sanity check to estimate relatively small SiC mirror cost versus aperture size and quality, the cost of modest size glass mirrors is used along with the 5% scaling factor (i.e. 20X lower removal rate during polishing) for SiC

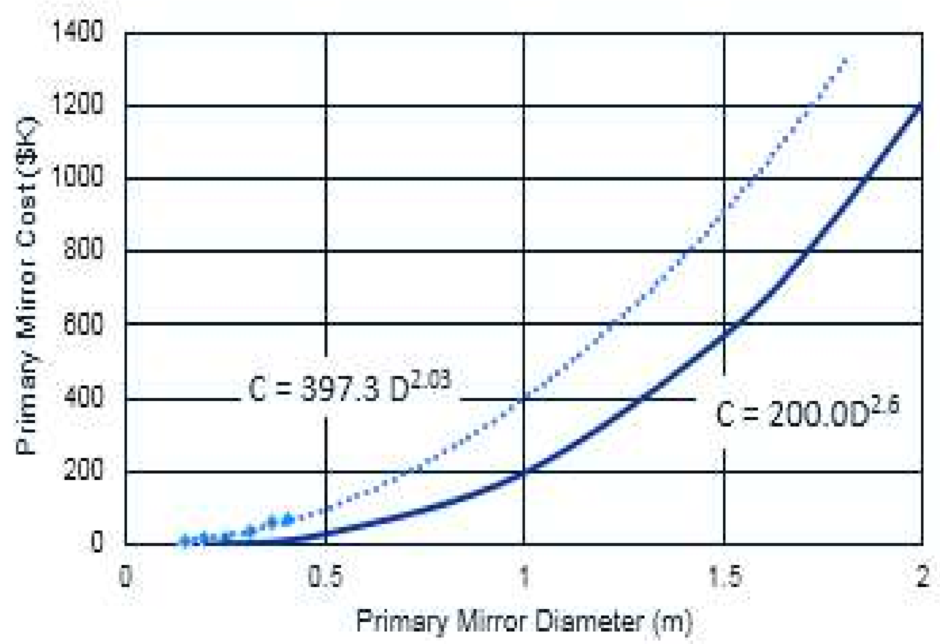

Mirror cost based on equation (1) (solid line) compared to data extrapolated from small glass mirrors and scaled to reflect the added complexity of SiC processing (dashed line) in $K.

- The small mirror power law curve indicates a roughly 25% higher cost in the region of interest.

Conclusions

- Based on the initial conclusion that an array of 141, 1.01 m diameter mirrors is nearly optimal, the cost of the array should be bounded by:

$$C_H = q\left[(0.397)\cdot\left(\frac{D}{\sqrt{q}}\right)^{2.03} + .47\cdot q^{-0.33} + \left[\frac{D}{\sqrt{q}}\cdot\left(\frac{D}{\sqrt{q}}\cdot .035 - 0.026\right) + .012\right]\right] \quad (18)$$

on the high side. Using this equation, the projected total array cost is $73 M, with $57 M, $13 M and $ 3 M attributed to the telescopes, refrigerators and domes, respectively.

- Equation [5] or Figure 11 can be used to trade cost of the highly polished SiC mirror with a less perfect but somewhat larger mirror. For example, instead of polishing to a micro-roughness of λ/100, a **1.92 m mirror with a λ/10 micro-roughness** could be used (assuming a correlation of 0.25 is feasible), enabling a ≈3X reduction in post-polishing costs. This implies an **initial investment of about $ 55 M for the optical ground array,** and a 25 year life-cycle cost of about $ 85 M.

- Finally, consider an optimal mirror scaled from a nominal 1.3 m SiC mirror (assuming feasibility from a manufacturing perspective and turbulence issues). The **scaled mirror would be ≈2.5 m in diameter** and the **upper cost is slightly lower – about $ 51 M**. In this case, $38.4 M, $9.2 M and $ 3.2 M are attributed to the telescopes, refrigerators and domes, respectively. And, only 85 telescopes are required. 2.5 m is considered to be an upper limited on SiC mirror manufacturing technology.

- These costs can be further reduced by dedicating one refrigerator to multiple channels (detectors). There is precedent to suggest that at least 8 single photon detector channels can be accommodated by a single refrigerator.

NASA's Deep Space Network

(Goldstone CA, Canberra Australia and Madrid Spain)

Next steps…

Insert an X-band SQIF into the 34 m DSS_13 antenna at Goldstone!

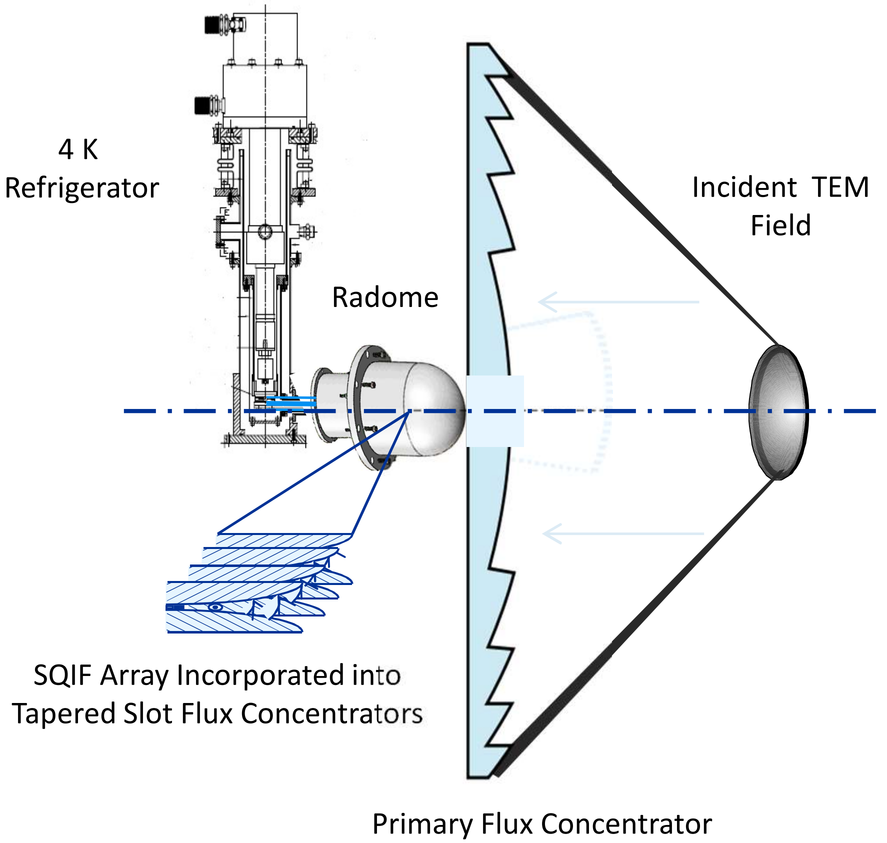

References

1. "A Cost-Performance Model for Ground-Based Optical Communications Receiving Telescopes," J. R. Lesh and D. L. Robinson, *The Telecommunications and Data Acquisition Progress Report 42-87, July–September 1986*, Jet Propulsion Laboratory, Pasadena, California, pp 56–64, November 15, 1986. http://ipnpr.jpl.nasa.gov/progress_report/
2. "Deep Space Optical Communications," Hamid Hemmati, Editor, Jet Propulsion Laboratory California Institute of Technology, Deep Space Communications and Navigation Series October, 2005.
3. "Low Temperature Electronics: Physics, Devices, Circuits and Applications," E. Gutierrez, M. Deen and C. Claeys eds., Academic Press, 2001, pp. 932-933.
4. Ibid.
5. "Deep Space Optical Communications," Hamid Hemmati, Editor, Jet Propulsion Laboratory California Institute of Technology, Deep Space Communications and Navigation Series October, 2005, pp. 480
6. "The Scaling Relationship Between Telescope Cost And Aperture Size For Very Large Telescopes," Gerard T. van Belle ; Aden B. Meinel and Marjorie P. Meinel, *Proc. SPIE* 5489, Ground-based Telescopes, 563 (September 28, 2004).
7. http://www.optcorp.com/tt-pd15-pro-dome-15-observatory.html
8. Personal Communication, Paul Shubert (Schafer), July 10, 2015.
9. "Antenna Tolerance Theory," J. Ruze, Proc. IEEE, Vol. 54, pp. 633-640, April, 1966.
10. "Deep-Space Optical Reception Antenna (DSORA): Aperture Versus Quality," J. Sandusky, D. Hoppe, and M. Britcliffe, TMO Progress Report 42-143, November 15, 2000.
11. "The Effect of Boundary Support and Reflector Dimensions on Inflatable Parabolic Antenna Performance," M. Coleman, F. Baginski and R. Romanofsky, NASA TM 2011-217110, November, 2011.
12. "Total Integrated Scatter from Surfaces with Arbitrary Roughness, Correlation Widths, and Incident Angles," J. Harvey et al. Optical Engineering, Vol. 51, January 2012.
13. "Ground Based Astronomy A Ten Year Program," National Academy of Sciences – National Research Council, Washington, DC, 1964.
14. Personal Communication, Matthew Shaw (JPL), February 26, 2015.
15. An Analytical and Experimental Procedure for Determining the mm-Wave Propagation Characteristics of GaAs Microstrip Lines," Romanofsky, R. R., NASA TP-2899, 1989.
16. Correction Factor for Determining the London Penetration Depth from Strip Resonators," R.R. Romanofsky, IEEE Trans. Applied Superconductivity, Vol.8, No. 1, March 1998
17. Quantum Sensitivity – Superconducting Quantum Interference Filter-Based Microwave Receivers" by O. Mukhanov, G. Prokopenko, and R. Romanofsky, IEEE Microwave Magazine, Sept/Oct 2014, pp.57-65